Giant anisotropy of magnetic damping and significant in-plane uniaxial magnetic anisotropy in amorphous $Co_{40}Fe_{40}B_{20}$ films on GaAs(001)*

Ji Wang(王佶)[1], Hong-Qing Tu(涂宏庆)[1,2], Jian Liang(梁健)[3], Ya Zhai(翟亚)[3], Ruo-Bai Liu(刘若柏)[1], Yuan Yuan(袁源)[1], Lin-Ao Huang(黄林傲)[1], Tian-Yu Liu(刘天宇)[1], Bo Liu(刘波)[4,†], Hao Meng(孟皓)[4], Biao You(游彪)[1,6], Wei Zhang(张维)[1,6], Yong-Bing Xu(徐永兵)[5], and Jun Du(杜军)[1,6,‡]

[1] *National Laboratory of Solid State Microstructures and Department of Physics, Nanjing University, Nanjing* 210093, *China*
[2] *Department of Mathematics and Physics, Nanjing Institute of Technology, Nanjing* 211167, *China*
[3] *Department of Physics and Jiangsu Key Laboratory of Advanced Metallic Materials, Southeast University, Nanjing* 211189, *China*
[4] *Key Laboratory of Spintronics Materials, Devices and Systems of Zhejiang Province, Hangzhou* 311300, *China*
[5] *Department of Electronic Engineering, Nanjing University, Nanjing* 210093, *China*
[6] *Collaborative Innovation Center of Advanced Microstructures, Nanjing* 210093, *China*

(Received 5 July 2020; revised manuscript received 31 July 2020; accepted manuscript online 7 August 2020)

Tuning magnetic damping constant in dedicated spintronic devices has important scientific and technological implications. Here we report on anisotropic damping in various compositional amorphous CoFeB films grown on GaAs(001) substrates. Measured by a vector network analyzer-ferromagnetic resonance (VNA-FMR) equipment, a giant magnetic damping anisotropy of 385%, i.e., the damping constant increases by about four times, is observed in a 10-nm-thick $Co_{40}Fe_{40}B_{20}$ film when its magnetization rotates from easy axis to hard axis, accompanied by a large and pure in-plane uniaxial magnetic anisotropy (UMA) with its anisotropic field of about 450 Oe. The distinct damping anisotropy is mainly resulted from anisotropic two-magnon-scattering induced by the interface between the ferromagnetic layer and the substrate, which also generates a significant UMA in the film plane.

Keywords: magnetic damping, uniaxial magnetic anisotropy, ferromagnetic resonance, two-magnon scattering

PACS: 75.78.−n, 75.30.Gw, 76.50.+g **DOI:** 10.1088/1674-1056/abad1d

1. Introduction

Magnetic damping constant α plays an important role in magnetic precession and spin relaxation process in spintronic devices.[1–7] During magnetization switching, α essentially determines the speed of magnetization reversal, hence one can substantially reduce the switching time by increasing α.[4,5] Moreover, the critical current density of spin-transfer-torque (STT) switching is found to be proportional to α.[6,7] Therefore, tuning α to an appropriate value is of great importance to develop high performance spintronic devices. Intensive efforts have been devoted to effective modification of α, e.g., alter the thickness[8] or composition[9] of the ferromagnetic (FM) layer, change the capping layer,[10] modify the interface,[11] incorporate the dopants into the FM layer,[12] and so on, but it remains difficult to manipulate α in a single dedicated device. Although tuning α through spin torque has been demonstrated as an effective approach,[13,14] its volatile nature and the required large current density place strong hurdles for practical applications.

Recently, several groups[15–21] reported anisotropic damping in the film plane, i.e., α could be tuned via rotating the magnetization orientation of the FM layer in the same sample. Meanwhile, the anisotropic damping is found to be accompanied with prominent in-plane magnetic anisotropies in the FM layer, e.g., twofold uniaxial magnetic anisotropy (UMA), fourfold magneto-crystalline anisotropy (MCA), or both of them. For the convenience of comparison, a damping anisotropy constant (η) is defined as $\eta = [\alpha(\text{maximum})/\alpha(\text{minimum}) - 1] \times 100\%$. Chen *et al.*[15] reported an anisotropic Gilbert damping with a significant UMA in the Fe/GaAs(001) system, however, η is only about 20%. They attributed the damping anisotropy to anisotropic density of state at the Fermi level. Li *et al.*[16] reported a giant Gilbert damping anisotropy with a maximum–minimum ratio of 400% (i.e., $\eta = 300\%$) in the CoFe/MgO(100) system. This damping anisotropy is found to be accompanied with an obvious MCA and its mechanism is attributed to the variation of spin–orbit coupling for different magnetization orientations. In contrast to the results in Ref. [15], for the same Fe/GaAs(001) sys-

*Project supported by the National Key Research and Development Program of China (Grant No. 2016YFA0300803), the National Natural Science Foundation of China (Grant Nos. 51971109, 51771053, and 51471085), and Scientific Research Foundation of Nanjing Institute of Technology (Grant Nos. ZKJ201708 and CKJB201708).

†Corresponding author. E-mail: liubo@hikstor.com
‡Corresponding author. E-mail: jdu@nju.edu.cn

tem, Yang *et al.*[17] reported that η could be increased to 66%. They claimed that the damping anisotropy is correlated to the in-plane UMA of the Fe film which originates from the interfacial effect between Fe and GaAs. The anisotropic magnetic damping has also been observed in some other magnetic alloy films, such as Co_2FeAl,[18] Co_2FeSi,[19] Co_2MnSi,[20] and FeGa.[21] However, in all these studies, the FM layers are either single-crystalline or highly textured polycrystalline. Since MCA can be completely ruled out, amorphous FM film (e.g., CoFeB) has been found to exhibit a pure in-plane UMA after being deposited on an appropriate substrate (e.g., GaAs).[22,23] Although the mechanism responsible for such UMA remains not fully resolved, it is well recognized that the UMA originates from the interfacial interaction between the FM layer and the substrate.[22,23]

Very recently, we reported an anisotropic magnetic damping accompanied with a pure in-plane UMA in amorphous $Co_{56}Fe_{24}B_{20}$ film deposited on GaAs(001) substrate, which is explained by anisotropic two-magnon scattering (TMS).[24] However, the largest values of UMA field and η could only reach $\sim$ 200 Oe and 109%, respectively. Since both magnetic damping and magnetic anisotropy are closely related to the composition of magnetic alloy,[9,25,26] in this work, we aim to enhance the damping anisotropy by changing the relative composition between Co and Fe while maintaining the B content in various amorphous CoFeB films. Remarkably, the largest tuning effect has been achieved in a 10-nm-thick $Co_{40}Fe_{40}B_{20}$ film deposited on GaAs(001) substrate for which η could be increased substantially to 385% with the UMA field $\sim$ 450 Oe.

2. Experimental details

The commercial GaAs(001) wafers were diced into about 4 mm $\times$ 4 mm pieces as substrates. Each of them is in rectangular shape with one edge along [110] and the other along [1$\bar{1}$0] direction. Before deposition of CoFeB films, the substrates need to be etched and cleaned by proper process. Detailed descriptions of the GaAs wafer parameters and the etching/cleaning procedures can be found in previous reports.[27,28] Three sets of CoFeB films with different compositions, i.e., $Co_{20}Fe_{60}B_{20}$, $Co_{40}Fe_{40}B_{20}$, and $Co_{56}Fe_{24}B_{20}$, were deposited onto the GaAs substrates by dc magnetron sputtering at normal incidence from the corresponding commercial CoFeB alloy targets. The chamber base pressure was lower than 8.0×10^{-6} Pa and the Ar pressure was kept at 0.3 Pa during film deposition. Finally, a 2 nm Ta film was deposited as the capping layer to prevent the CoFeB film from oxidation. The crystalline structures of the CoFeB samples were characterized by x-ray diffraction (XRD, Bruker D8-Advance) with Cu K_α radiation. The in-plane magnetic hysteresis (M–H) loops were measured by a vibrating sample magnetometer (VSM, Microsense EV7). The magnetic dynamic properties were investigated by a home-made vector network analyzer-ferromagnetic resonance (VNA-FMR) equipment with the driving microwave frequency varied from 8 GHz to 18 GHz.

3. Results and discussion

Figure 1 shows the XRD patterns for the two films of GaAs/$Co_{40}Fe_{40}B_{20}$ (10 nm)/Ta (2 nm) and GaAs/$Co_{40}Fe_{40}B_{20}$ (20 nm)/Ta (2 nm), which are denoted as sample S1 and sample S2, respectively. From Fig. 1, it can be seen that the XRD patterns for these two samples are almost the same as that of the GaAs(001) substrate. The absence of diffraction peaks from Fe, Co, FeCo, and other alloys possibly formed indicates amorphous structure of the $Co_{40}Fe_{40}B_{20}$ films deposited on the GaAs(001) substrate. Similar results can also be observed for the $Co_{20}Fe_{60}B_{20}$ films (not shown here) and $Co_{56}Fe_{24}B_{20}$ films[24] with the same thicknesses.

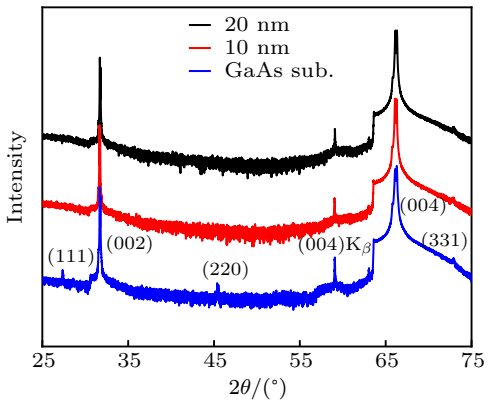

Fig. 1. XRD patterns for the $Co_{40}Fe_{40}B_{20}$ film samples and a pure GaAs(001) substrate.

The M–H loops measured along GaAs [110] and [1$\bar{1}$0] directions for samples S1 and S2 are displayed in Figs. 2(a) and 2(b), respectively. The nearly squared loops with low saturation fields in Fig. 2(a) and slant loops with high saturation fields in Fig. 2(b) indicate that the easy axis (EA) is along GaAs [110] while the hard axis (HA) is along GaAs [1$\bar{1}$0]. In Fig. 2(b), the saturation field along HA is $\sim$ 500 Oe for sample S1, which is much larger than $\sim$ 260 Oe for sample S2. At low fields, a kink (a small loop) appearing at the loop along EA (HA) may be caused by the complex magnetizing process due to the interfacial magnetic inhomogeneity between CoFeB and GaAs. In order to reveal the symmetry of the in-plane magnetic anisotropy for these two samples, the M–H loops were measured every 15° from the GaAs [110] direction. As shown in Fig. 2(c), the azimuthal dependence of M_R/M_S (i.e., the ratio between the remanent magnetization and the saturation magnetization) clearly shows that a pure UMA exists in the film plane for sample S1 or S2 with EA (HA) along GaAs [110] (GaAs [1$\bar{1}$0]).

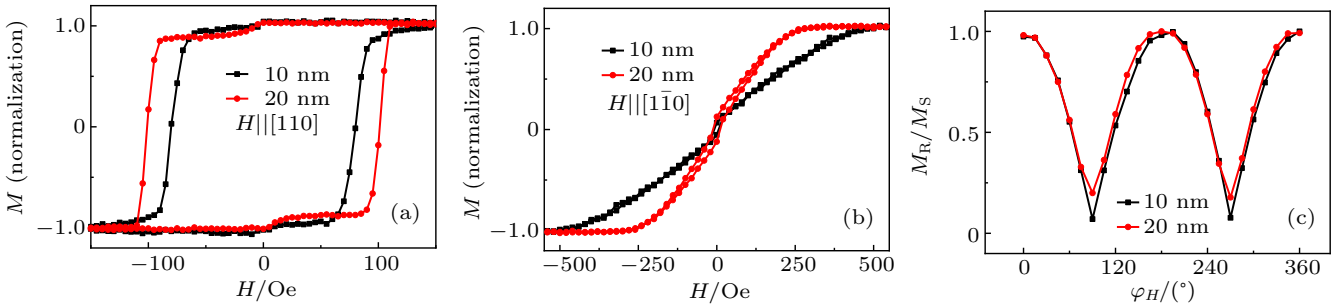

Fig. 2. The *M*–*H* loops measured along [110] (a) and [1$\bar{1}$0] (b) crystallographic orientations of the GaAs(001) substrate and the azimuthal dependence of remanence ratio (c) for samples S1 and S2.

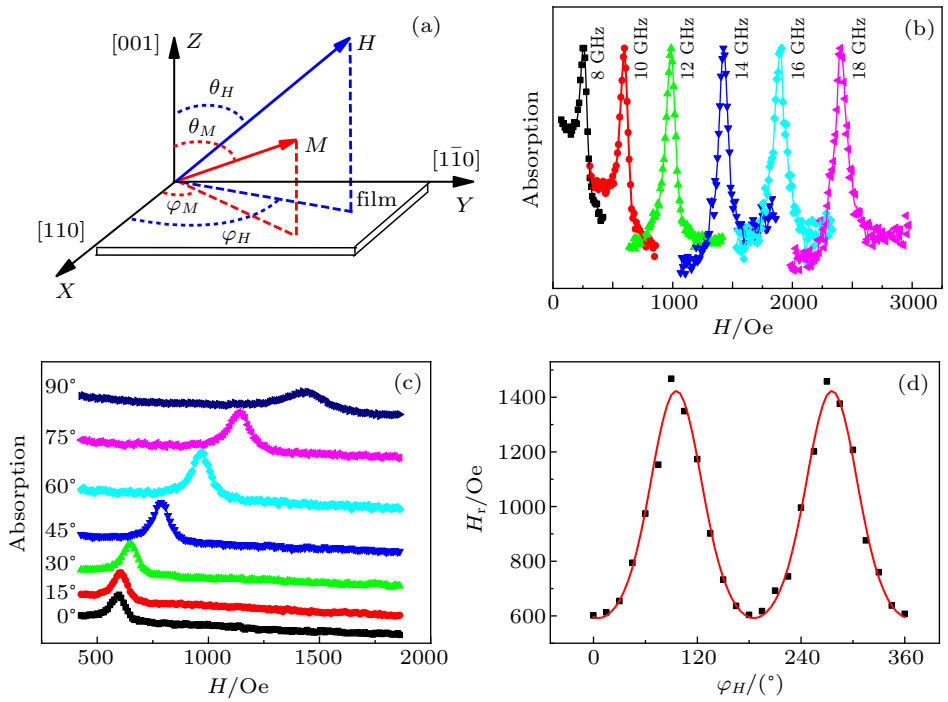

Fig. 3. (a) The measurement configuration of VNA-FMR. (b) Typical VNA-FMR spectra for several selected frequencies at $\varphi_H = 0°$. (c) Typical VNA-FMR spectra at various azimuthal angles recorded at $f = 10$ GHz. (d) The experimental (square dots) and fitted (red line) in-plane azimuthal dependence of H_r at $f = 10$ GHz.

In order to investigate the magnetic dynamic properties of the samples, VNA-FMR measurements were employed with the measurement configuration sketched in Fig. 3(a). H and M denote the external magnetic field and the magnetization, respectively. The azimuthal angle of H (M), i.e., φ_H (φ_M), denotes the angle rotating anticlockwise from GaAs [110] to the projection of H (M). For examples, $\varphi_H = 0°$ and 90° means that H is applied along GaAs [110] and GaAs [1$\bar{1}$0], respectively. θ_H (θ_M) denotes the angle between H (M) and the z-axis. In the present studies, because H is always applied in the film plane, we can obtain $\theta_H = \theta_M = 90°$. In the following, sample S1 will be selected as a representative sample to demonstrate the FMR results. Figures 3(b) and 3(c) exhibit the FMR spectra for sample S1 at varied frequencies along the EA ($\varphi_H = 0°$) and at varied azimuthal angles with a fixed frequency of 10 GHz, respectively. It can be seen clearly that the resonance field (peak position of H) moves towards high field side with increasing the driving frequency (see Fig. 3(b)) or changing the azimuthal angle φ_H from EA to HA (see Fig. 3(c)), and meanwhile the linewidth also increases monotonically. By fitting the FMR spectrum by symmetrical and asymmetric Lorentz lines,[29] the experimental values of both the resonance field H_r and the linewidth ΔH (full width at half maximum of the FMR spectrum) can be obtained.

The total free energy per unit volume can be written as[24]

$$\begin{aligned} F \;=\; & -HM_S[\sin\theta_M \sin\theta_H \cos(\varphi_H - \varphi_M) + \cos\theta_M \cos\theta_H] \\ & -(2\pi M_S^2 - K_P)\sin^2\theta_M - K_u \sin^2\theta_M \cos^2\varphi_M, \end{aligned} \tag{1}$$

where the first, second, and third terms denote the densities of Zeeman energy, effective demagnetized energy, and in-plane UMA energy, respectively. M_S, K_P, and K_u denote the saturate magnetization, out-of-plane and in-plane UMA energy constants, respectively. Note that the MCA has been neglected in the total energy. According to the Smit–Beljers equation,[30] the resonance equation for azimuthal rotation ($\theta_H = \theta_M = 90°$) can be derived to be[18,24]

$$\left(\frac{\omega}{\gamma}\right)^2 = [H_r\cos(\varphi_H-\varphi_M)+4\pi M_{eff}+H_u\cos^2\varphi_M] \times [H_r\cos(\varphi_H-\varphi_M)+H_u\cos(2\varphi_M)], \quad (2)$$

where ω is the circular frequency ($\omega = 2\pi f$), γ is the gyromagnetic ratio ($\gamma = g\mu_B/\hbar$, g is the Landé factor, μ_B is the Bohr magneton, $\hbar$ is the reduced Planck constant), H_r is the resonance field, H_u is the in-plane UMA field ($H_u = 2K_u/M_S$); $4\pi M_{eff} = 4\pi M_S - H_P$, $H_P = 2K_P/M_S$. As shown in Fig. 3(d), the experimental angular dependence of H_r at $f = 10$ GHz can be well fitted according to Eq. (2) and the minimum conditions of the total free energy, indicating a pure in-plane UMA for sample S1, which is in good consistent with the M_R/M_S results shown in Fig. 2(c). Similar results can be found at other frequencies for sample S1 and in other CoFeB samples with different thicknesses and compositions. By fitting calculations, the parameters of H_u, $4\pi M_{eff}$, and g for sample S1 can be obtained as 450 Oe, 9889 Oe, and 2.10, respectively. Note that the fitted value of H_u is close to the saturation field ($\sim$ 500 Oe) shown in Fig. 2(b), which further confirms the presence of a pure in-plane UMA in sample S1.

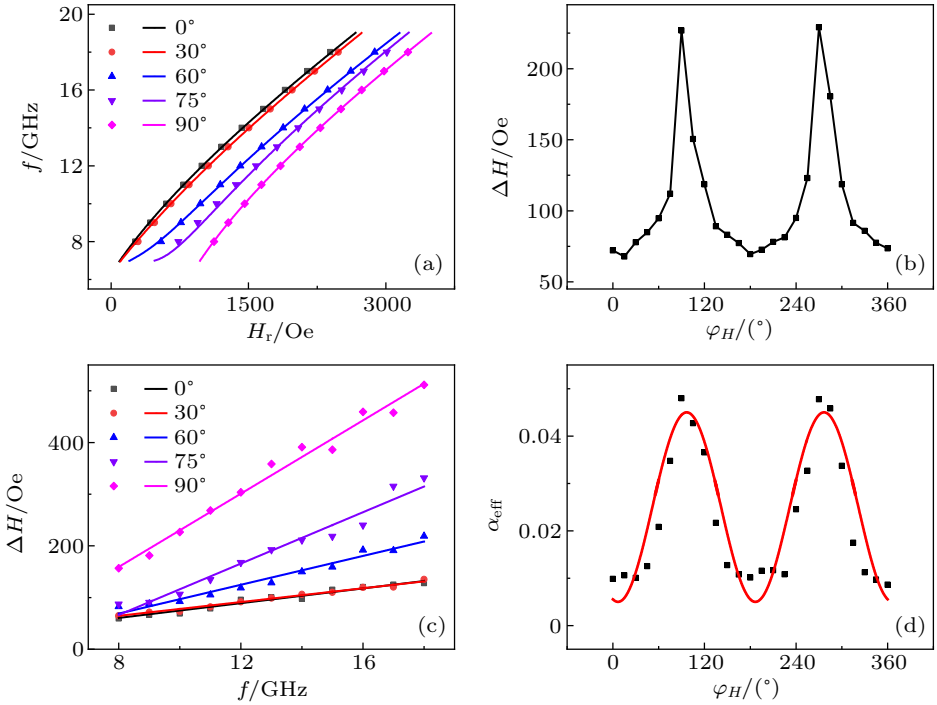

Fig. 4. (a) The H_r dependences of frequency at $\varphi_H = 0°$, 30°, 60°, 75°, 90°, (b) azimuthal dependence of ΔH at $f = 10$ GHz, (c) frequency dependences of ΔH at $\varphi_H = 0°$, 30°, 60°, 75°, 90°, and (d) azimuthal dependence of α_{eff} for sample S1. The experimental results are shown as dots and the fitted results are shown as lines except for (b), in which the line is only guide to eyes.

The experimental $f \sim H_r$ results at a fixed φ_H can be also fitted according to Eq. (2) and minimization of the energy. As shown in Fig. 4(a), the fitted results are in good consistent with the experimental ones at $\varphi_H = 0°$, 30°, 60°, 75°, 90° for sample S1. Similar results can be observed in all the other samples. Besides the resonance field H_r, the linewidth ΔH is another important parameter, which is much associated with the magnetic damping. Figure 4(b) shows the azimuthal dependence of ΔH at $f = 10$ GHz for sample S1, which demonstrates a clear twofold symmetry. Similar results can also be found at other frequencies and in all the other samples. The frequency dependent linewidth can be approximately written as[18]

$$\Delta H \approx \Delta H_0 + \left[\left(\alpha + \frac{\Gamma_0}{2M_{eff}}\right) + \frac{\Gamma_2}{2M_{eff}}\cos 2(\varphi_H - \varphi_2)\right]\frac{4\pi f}{\gamma} = \Delta H_0 + \alpha_{eff}\frac{4\pi f}{\gamma}, \quad (3)$$

where ΔH_0 is the linewidth independent of frequency known as the inhomogeneous broadening, which originates from magnetic inhomogeneity;[31] Γ_0, Γ_2, and φ_2 are induced from the expected twofold symmetry, α_{eff} is the effective damping coefficient and can be obtained from the slope of the frequency dependency of ΔH. As shown in Fig. 4(c), the experimental results of $\Delta H \sim f$ at various φ_H varied from 0° to 90° can be well fitted in a linear manner and thus the corresponding values of α_{eff} can be obtained from the slope. As shown in Fig. 4(d), after performing a 360° φ_H-scan at every 15° for measuring a $\Delta H \sim f$ curve, the experimental azimuthal dependence of α_{eff} (dots) is obtained, which can be fairly well fitted (solid line) according to Eq. (3). Figure 4(d) also exhibits that α_{eff} is anisotropic in the film plane and presents a twofold symmetry, similar to H_r and ΔH. Our previous studies[24] reveal that the magnetic damping anisotropy in CoFeB/GaAs(001) system mainly originates from the anisotropic strength of TMS, which is induced by the CoFeB–GaAs interface and behaves

the strongest (weakest) along the HA (EA), i.e., $[1\bar{1}0]$ ([110]) crystallographic orientation of the GaAs substrate. Moreover, the angular dependence of ΔH_0 (not shown here) also presents a nearly twofold symmetry with the absolute value of ΔH_0 to be the largest (smallest) along the HA (EA), implying that the magnetic nonuniformity is much more serious near the HA than that near the EA, which is consistent with the CoFeB–GaAs interface characterization results reported previously.[24]

According to the definition of η, it can be written as $\eta = [\alpha_{\rm eff}(90^\circ)/\alpha_{\rm eff}(0^\circ) - 1] \times 100\%$. The η values for all the films with different thicknesses and compositions are summarized in Table 1. It can be seen that η decreases with increasing the film thickness at the same composition, in consistent with that the magnetic damping anisotropy is interface induced. The 10-nm-thick $Co_{40}Fe_{40}B_{20}$ film has the largest η of 385%, which means that the damping constant increases by about four times when the sample is rotated from EA to HA. More interestingly, the sample also has the strongest UMA with $H_{\rm u}$ up to about 450 Oe, implying that the stronger the UMA is, the larger damping the anisotropy presents. According to directional ordering of atom pairs of Néel–Taniguchi theory,[32,33] the magnetization-induced UMA and its energy constant $K_{\rm u}$ in $Fe_{1-x}Co_x$ films can be estimated by $K_{\rm u} = ax^2(1-x)^2(T_{\rm C} - T_{\rm d})$.[23,25,26] Here, x is the atomic concentration of cobalt, $T_{\rm C}$ is the Curie temperature, $T_{\rm d}$ is the deposition or annealing temperature, and a is a constant. Based on this formula, ideally the maximum $K_{\rm u}$ appears when Co and Fe have equal compositions, which seems to be consistent with the present CoFeB/GaAs system.

Table 1. Magnetic damping constants at various azimuthal angles and the corresponding values of η in the CoFeB films with different compositions and thicknesses. The data for the $Co_{56}Fe_{24}B_{20}$ (10 nm) and $Co_{56}Fe_{24}B_{20}$ (20 nm) films are taken from Ref. [24].

Sample	0°	30°	60°	90°	η
$Co_{20}Fe_{60}B_{20}$ (10 nm)	0.0088 ± 0.0004	0.0089 ± 0.0004	0.0173 ± 0.0009	0.0343 ± 0.0009	290%
$Co_{20}Fe_{60}B_{20}$ (20 nm)	0.0086 ± 0.0003	0.0087 ± 0.0005	0.0121 ± 0.0005	0.0162 ± 0.0007	88%
$Co_{40}Fe_{40}B_{20}$ (10 nm)	0.0099 ± 0.0005	0.0100 ± 0.0005	0.0208 ± 0.0009	0.0480 ± 0.0009	385%
$Co_{40}Fe_{40}B_{20}$ (20 nm)	0.0087 ± 0.0003	0.0089 ± 0.0003	0.0142 ± 0.0003	0.0190 ± 0.0007	118%
$Co_{56}Fe_{24}B_{20}$ (10 nm)	0.0116 ± 0.0003	0.0124 ± 0.0005	0.0192 ± 0.0009	0.0242 ± 0.0009	109%
$Co_{56}Fe_{24}B_{20}$ (20 nm)	0.0103 ± 0.0005	0.0104 ± 0.0005	0.0141 ± 0.0005	0.0151 ± 0.0005	47%

4. Conclusions

In summary, a distinct magnetic damping anisotropy accompanied with a strong and pure in-plane UMA was found in amorphous CoFeB films with different compositions when they were deposited on GaAs(001) substrates. The largest damping anisotropy and UMA field of 385% and ~ 450 Oe, respectively, have been obtained in a 10-nm-thick $Co_{40}Fe_{40}B_{20}$ film. Both the damping anisotropy and UMA exhibit similar composition and thickness dependences, indicating that they may have the same origin stemming from interfacial interactions. Our findings clearly demonstrate that the magnetic damping can be continuously tuned via rotating the magnetization orientation within a sample, which paves the way to developing new-generation spintronic devices with optimized dynamic properties.

References

[1] Hals K M D, Flensberg K and Rudner M S 2015 *Phys. Rev. B* **92** 094403

[2] Žutić I, Fabian J and Sarma S D 2004 *Rev. Mod. Phys.* **76** 323

[3] Li S F, Cheng C Y, Meng K K and Chen C L 2019 *Chin. Phys. B* **28** 097502

[4] Ma T Y, Luo Z, Li Z W, Qiao L, Wang T and Li F S 2019 *Chin. Phys. B* **28** 057505

[5] Benakli M, Torabi A F, Mallary M L, Zhou H and Bertram H N 2001 *IEEE Trans. Magn.* **37** 1564

[6] Li X, Zhang Z Z, Jin Q Y and Liu Y W 2009 *New J. Phys.* **11** 023027

[7] Costa J D, Serrano-Guisan S, Lacoste B, Jenkins A S, Böhnert T, Tarequzzaman M, Borme J, Deepak F L, Paz E, Ventura J, Ferreira R and Freitas P P 2017 *Sci. Rep.* **7** 7237

[8] Liu X Y, Zhang W Z, Carter, M J and Xiao G 2011 *J. Appl. Phys.* **110** 033910

[9] Schoen M A W, Thonig D, Schneider M L, Silva T J, Nembach H T, Eriksson O, Karis O and Shaw J M 2016 *Nat. Phys.* **12** 839

[10] Azzawi S, Ganguly A, Tokaç M, Rowan-Robinson R M, Sinha J, Hindmarch A T, Barman A and Atkinson D 2016 *Phys. Rev. B* **93** 054402

[11] Urban R, Woltersdorf G and Heinrich B 2001 *Phys. Rev. Lett.* **87** 217204

[12] Luo C, Feng Z, Fu Y, Zhang W, Wong P K J, Kou Z X, Zhai Y, Ding H F, Farle M, Du J and Zhai H R 2014 *Phys. Rev. B* **89** 184412

[13] Ando K, Takahashi S, Harii K, Sasage K, Ieda J, Maekawa S and Saitoh E 2008 *Phys. Rev. Lett.* **101** 036601

[14] Liu L Q, Moriyama T, Ralph D C and Buhrman R A 2011 *Phys. Rev. Lett.* **106** 036601

[15] Chen L, Mankovsky S, Wimmer S, Schoen M A W, Körner H S, Kronseder M, Schuh D, Bougeard D, Ebert H, Weiss D and Back C H 2018 *Nat. Phys.* **14** 490

[16] Li Y, Zeng F L, Zhang S S L , Shin H, Saglam H, Karakas V, Ozatay O, Pearson J E, Heinonen O G, Wu Y Z, Hoffmann A and Zhang W 2019 *Phys. Rev. Lett.* **122** 117203

[17] Yang L, Yan Y, Chen Y Q, Chen Y Y, Liu B, Chen Z D, Lu X Y, Wu J, He L, Ruan X Z, Liu B and Xu Y B 2020 *J. Phys. D: Appl. Phys.* **53** 115004

[18] Chen Z D, Kong W W, Mi K, Chen G L, Zhang P, Fan X L, Gao C X and Xue D S 2018 *Appl. Phys. Lett.* **112** 122406

[19] Kasatani Y, Yamada S, Itoh H, Miyao M, Hamaya K and Nozaki Y 2014 *Appl. Phys. Express* **7** 123001

[20] Yilgin R, Sakuraba Y, Oogane M, Mizukami S, Ando Y and Miyazaki T 2007 *Jpn. J. Appl. Phys.* **46** L205

[21] Li Y, Li Y, Liu Q, Yuan Z, Zhan Q F, He W, Liu H L, Xia K, Yu W, Zhang X Q and Cheng Z H 2019 *New J. Phys.* **21** 123001

[22] Hindmarch A T, Kinane C J, MacKenzie M, Chapman J N, Henini M, Taylor D, Arena D A, Dvorak J, Hickey B J and Marrows C H 2008 *Phys. Rev. Lett.* **100** 117201
[23] Hindmarch A T, Rushforth A W, Campion R P, Marrows C H and Gallagher B L 2011 *Phys. Rev. B* **83** 212404
[24] Tu H Q, Wang J, Huang Z C, Zhai Y, Zhu Z D, Zhang Z Z, Qu J T, Zheng R K, Yuan Y, Liu R B, Zhang W, You B and Du J 2020 *J. Phys: Condens. Matter* **32** 335804
[25] Srivastava R S 1977 *J. Appl. Phys.* **48** 1355
[26] Ohodnicki P R, McHenry M E and Laughlin D E 2007 *J. Appl. Phys.* **101** 09N118
[27] Tu H Q, You B, Zhang Y Q, Gao Y, Xu Y B and Du J 2015 *IEEE Trans. Magn.* **51** 2005104
[28] Tu H Q, Liu B, Huang D W, Ruan X Z, You B, Huang Z C, Zhai Y, Gao Y, Wang J, Wei L J, Yuan Y, Xu Y B and Du J 2017 *Sci. Rep.* **7** 43971
[29] Qiao S, Nie S H, Zhao J H, Huo Y, Wu Y Z and Zhang X H 2013 *Appl. Phys. Lett.* **103** 152402
[30] Smit J and Beljers H G 1955 *Philips Res. Rep.* **10** 113
[31] Arias R and Mills D L 1999 *Phys. Rev. B* **60** 7395
[32] Néel L 1954 *J. Phys. Radium* **15** 225
[33] Taniguchi S 1955 *Sci. Rep. Res. Inst. Tohoku Univ. Ser. A* **7** 269